JOURNAL OF GUIDANCE, CONTROL, AND DYNAMICS
Vol. 30, No. 5, September–October 2007

Discrete-Time, Closed-Loop Aeromechanical Stability Analysis of Helicopters with Higher Harmonic Control

Marco Lovera* and Patrizio Colaneri†
Politecnico di Milano, 20133 Milano, Italy
and
Carlos Malpica‡ and Roberto Celi§
University of Maryland, College Park, Maryland 20742

DOI: 10.2514/1.13874

This paper presents an aeromechanical closed-loop stability and response analysis of a hingeless rotor helicopter with a higher harmonic control system for vibration reduction. The analysis includes the rigid body dynamics of the helicopter and blade flexibility. The gain matrix is assumed to be fixed and computed offline. The discrete elements of the higher harmonic control loop are rigorously modeled, including the presence of two different time scales in the loop. By also formulating the coupled rotor-fuselage dynamics in discrete form, the entire coupled helicopter higher harmonic control system could be rigorously modeled as a discrete system. The effect of the periodicity of the equations of motion is rigorously taken into account by converting the system into an equivalent system with constant coefficients and identical stability properties using a time-lifting technique. The most important conclusion of the present study is that the discrete elements in the higher harmonic control loop must be modeled in any higher harmonic control analysis. Not doing so is unconservative. For the helicopter configuration and higher harmonic control structure used in this study, an approximate continuous modeling of the higher harmonic control system indicates that the closed-loop, coupled helicopter higher harmonic control system is always stable, whereas the more rigorous discrete analysis shows that closed-loop instabilities can occur. The higher harmonic control gains must be reduced to account for the loss of gain margin brought about by the discrete elements. Other conclusions of the study are 1) the higher harmonic control is effective in quickly reducing vibrations, at least at its design condition; 2) a linearized model of helicopter dynamics is adequate for higher harmonic control design, as long as the periodicity of the system is correctly taken into account, that is, periodicity is more important than nonlinearity, at least for the mathematical model used in this study; and 3) when discrete and continuous systems are both stable, the predicted higher harmonic control control harmonics are in good agreement, although the initial transient behavior can be considerably different.

Nomenclature

$A(t)$	=	state matrix
$B(t)$	=	input (or control) matrix
$C(t)$	=	output (or measurement) matrix
$D(t)$	=	direct input/output matrix
k	=	discrete-time variable associated with T (1/rev dynamics)
N	=	number of rotor blades
n	=	number of acceleration measurements
n_s	=	number of acceleration (output) samples per revolution, $n_s = T/P$
P	=	acceleration (output) sampling interval, $P = T/n_s$
p	=	total number of outputs, $p = 2n$
R	=	control weighting matrix in HHC performance index
r	=	tuning parameter in HHC performance index
T	=	rotor revolution period, $T = 2\pi/\Omega$
T_C	=	HHC gain matrix
t	=	time (continuous)
$\mathbf{u}$	=	input (or control) vector
$\mathbf{u}_{\text{FCS}}$	=	pilot or flight control system input
$\mathbf{u}_{\text{HHC}}$	=	HHC input
W	=	output weighting matrix in HHC performance index
$\mathbf{x}$, $\mathbf{y}$	=	state and output vectors
$\mathbf{y}^i_{Nc}$, $\mathbf{y}^i_{Ns}$	=	N/rev cosine and sine harmonic of ith acceleration measurement (output)
η	=	discrete-time variable associated with P (acceleration sampling)
θ_{kc}, θ_{ks}	=	k/rev cosine and sine harmonic of pitch control input
Φ	=	state transition matrix
ψ	=	azimuth angle of reference blade, $\psi = \Omega t$
Ω	=	rotor angular velocity

Subscripts

$()_C$	=	quantity in the controller model
$()_F$	=	quantity in the harmonic analyzer model
$()_H$	=	quantity in the helicopter dynamic model
$()_{\text{lift}}$	=	time-lifted quantity
$()_Z$	=	quantity in the zero-order-hold model

Superscript

$\bar{()}$	=	discrete-time counterpart of continuous-time signal

Received 29 September 2005; revision received 8 June 2006; accepted for publication 8 June 2006.

*Associate Professor, Dipartimento di Elettronica e Informazione; lovera@elet.polimi.it.

†Professor, Dipartimento di Elettronica e Informazione; colaneri@elet.polimi.it.

‡Graduate Research Assistant, Department of Aerospace Engineering; cmalpica@eng.umd.edu.

§Professor, Department of Aerospace Engineering; celi@eng.umd.edu.

Introduction

HIGHER harmonic control (HHC) is an active vibration control technology that tries to reduce the vibratory components in the fuselage at the frequency of N-per-revolution (or N/rev, N being the number of rotor blades) by adding higher harmonic components to

the rotor controls. Amplitude and phase of these harmonics are determined online by a suitable control law. If the higher harmonic inputs are applied in the rotating system, via rotating high-frequency actuators, the technique is usually called individual blade control (IBC). IBC and HHC are generally considered as effective techniques for vibration reduction, although issues of power requirements and reliability have until now prevented widespread application on production helicopters [1].

HHC has been the subject of extensive research over the last three decades. The research until 1982 was reviewed by Johnson [2] as part of an extensive study of several types of HHC algorithms and implementation techniques that remain relevant to this date. More recent survey papers have been written by Friedmann and Millott [3] and Teves et al. [4]. Although HHC is generally studied in the context of rotor control, the basic HHC algorithm has also been successfully used for fuselage-mounted active vibration reduction [5].

Figure 1 shows a typical architecture of an HHC system. Although this is not the only possible architecture, nor is it necessarily the best, it is important for historical and practical reasons, and has been extensively studied theoretically and experimentally (e.g., [6]). Some helicopter outputs, typically N/rev components of fuselage vibrations, are extracted through a harmonic analysis and fed to a controller that computes appropriate values of the higher harmonic outputs, which are then injected into the rotor controls. Figure 2 depicts a hypothetical situation in which the HHC system is inoperative over the first quarter of the revolution of a reference blade, samples the desired output over the next quarter to build the desired harmonics to attenuate, computes the required inputs over the next half revolution, and updates the HHC inputs at the end of the revolution. These steps are not instantaneous, but are carried out over finite time intervals, and therefore cannot be rigorously described in state-space form.

This modeling problem is the probable reason why, although the basic characteristics of HHC algorithms have been investigated extensively, the influence of the aeromechanic behavior of the entire helicopter on the performance and, especially, the stability of the HHC system has been typically ignored. The helicopter dynamics have only been considered indirectly, through their contribution to the gain, or T, matrix. Stability analyses have focused on the stability of the HHC update algorithm, with or without online identification, not on the closed-loop stability of the complete helicopter with the HHC system turned on. Also, no study on the potential interactions between an HHC system and a flight control system (FCS) was available in the literature. These analyses require mathematical representation in state-space form, preferably with constant coefficients.

Some recent studies have addressed this gap. Cheng et al. [7] extracted a linearized, state-space, time-invariant model of the helicopter, and used it for a study of the interaction between the HHC and the flight control system. The harmonic analyzer is essentially modeled as if it were an analog analyzer, continuously extracting the required N/rev vibration harmonics. The computation delays are modeled using Padè approximants and the HHC input is updated continuously. The gain matrix T is fixed. One important conclusion is that while the HHC has little influence on the flight control system and on the handling qualities, the reverse is not true. There is a significant effect of maneuvers on vibration, which leads to higher required crossover frequencies for the HHC loop.

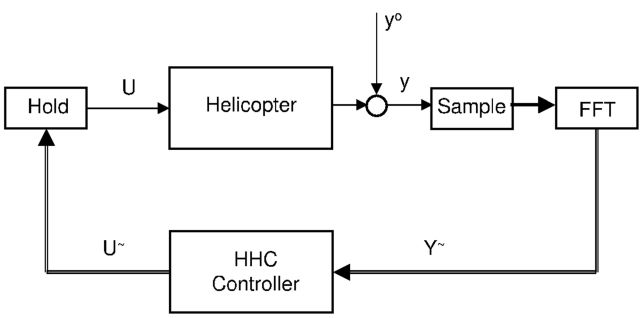

Fig. 1 Block diagram of a HHC loop (thin lines: continuous signals; thick lines: "fast sampling" discrete signals; double lines: 1/rev sampling signals).

Lovera et al. [8] studied the closed-loop stability of a hingeless rotor helicopter equipped with an HHC system. The T matrix is constant, and the HHC algorithm is written as a linear time-invariant dynamic compensator using the technique developed by Wereley and Hall [9], extended to cover inputs and outputs at different harmonics. This compensator is coupled to a high-order, coupled rotor-fuselage model, and the closed-loop stability is studied using Floquet theory and constant-coefficient approximations. The key results of the study are that 1) the HHC system does not degrade the aeromechanic stability, 2) the time constants of the HHC are such that interactions with a flight control system could occur, and 3) that the effects of periodic coefficients need to be taken into account.

A gap in the analysis of HHC systems, however, remains open, because the issues related to the actual discrete-time implementation were not included in [8] and have never been studied in detail in the literature. Discrete-time issues are likely to play a major role in determining the closed-loop behavior of the system. In fact, the typical update frequency for HHC control inputs is 1/rev, which is comparable with the bandwidth of the dynamics of the open loop, that is, uncontrolled helicopter rotor. Previous work on this problem (see, e.g., [8–10]) tried to overcome this difficulty by developing continuous-time, time domain counterparts of the discrete elements. On the other hand, a more complete and rigorous picture of the operation of HHC can be obtained by looking at the entire control loop, including the coupled rotor-fuselage dynamics, in discrete time rather than in continuous time.

In light of the preceding discussion, this paper has the following objectives:

1) to describe a typical discrete-time HHC architecture and derive suitable linearized, state-space, discrete models for all the components present in the control loop;

2) to formulate a coupled helicopter-HHC discrete model and convert it from a periodic, multiple sampling rate model to a constant-coefficient, single sampling rate model using time-lifting techniques; and

3) to perform a closed-loop, aeromechanic stability and response analysis of the discrete-time, coupled helicopter-HHC model, and compare it with the corresponding results obtained using a continuous-time model.

Finally, note that in this paper some additional simplifying assumptions are made, namely, 1) only the *nominal* stability of the HHC control loop will be studied, that is, it will be assumed that the T matrix is exactly known; 2) the T matrix is assumed to remain constant with speed and flight condition; and 3) no displacement or rate saturation of the HHC actuators occurs. Most of the proposed HHC implementations rely on the online identification of the T matrix to account for modeling errors, variations with flight conditions, and, to some extent, saturation. Therefore, the present paper should be considered as only a first step toward a complete, rigorous analysis of adaptive HHC solutions.

Helicopter Model

The baseline simulation model used in this study is a nonreal-time, blade element type, coupled rotor-fuselage simulation model. The model is discussed in detail in [11], and only a brief description will be provided here. The fuselage is assumed to be rigid and dynamically coupled with the rotor. A total of nine states describe fuselage motion through the nonlinear Euler equations. Fuselage and blades aerodynamics are described through tables of aerodynamic coefficients, and no small angle assumption is required. A coupled flap–lag–torsion elastic rotor model is used [12,13]. Blades are modeled as Bernoulli–Euler beams. The rotor is discretized using finite elements, with a modal coordinate transformation to reduce the number of degrees of freedom. The elastic deflections are not required to be small. Blade element theory is used to obtain the aerodynamic characteristics on each blade section. Quasi-steady aerodynamics is used, with a 3-state dynamic inflow model. The

complete dynamic system is modeled as a set of nonlinear ordinary differential equations written in implicit form [14].

The trim procedure is the same as in [15]. The rotor equations of motion are transformed into a system of nonlinear algebraic equations using a Galerkin method. The algebraic equations enforcing force and moment equilibrium, the Euler kinematic equations, the inflow equations, and the rotor equations are combined in a single coupled system. The solution yields the harmonics of a Fourier expansion of the rotor degrees of freedom, the pitch control settings, trim attitudes and rates of the entire helicopter, and main and tail rotor inflow.

Linearized models are extracted numerically, by perturbing rotor, fuselage, and inflow states about a trimmed equilibrium position. The resulting continuous-time, linearized, time-periodic model of the helicopter is in the form

$$\begin{cases} \dot{\mathbf{x}}_H(t) = A_H(t)\mathbf{x}_H(t) + B_{\mathrm{FCS}}(t)\mathbf{u}_{\mathrm{FCS}}(t) + B_{\mathrm{HHC}}(t)\mathbf{u}_{\mathrm{HHC}}(t) \\ \mathbf{y}_H(t) = C_H(t)\mathbf{x}_H(t) + D_{\mathrm{FCS}}(t)\mathbf{u}_{\mathrm{FCS}}(t) + D_{\mathrm{HHC}}(t)\mathbf{u}_{\mathrm{HHC}}(t) \end{cases} \tag{1}$$

where all the matrices are periodic, with a period corresponding to N/rev; the control vectors $\mathbf{u}_{\mathrm{FCS}}(t)$ and $\mathbf{u}_{\mathrm{HHC}}(t)$ are defined as in Eqs. (4) and (5), later in this section, while the outputs are the body frame accelerations measured by the control system.

The matrices of the linearized model are generated as a Fourier series. For example, the state matrix $A_H(\psi)$ is given as

$$A_H(\psi) = A_{H0} + \sum_{\ell=1}^{L} (A_{H\ell c}\cos \ell N\psi + A_{H\ell s}\sin \ell N\psi) \tag{2}$$

with $\psi = \Omega t$, and where the matrices A_{H0}, $A_{H\ell c}$, and $A_{H\ell s}$ are constant.

The control matrices $B_{\mathrm{FCS}}(\psi)$ and $B_{\mathrm{HHC}}(\psi)$ are obtained in the same Fourier series form as $A_H(\psi)$, Eq. (2), by assuming that the pitch control angle of the ith blade is given by

$$\begin{aligned} \theta_i(\psi) \quad &= \theta_0 + \theta_{1c}\cos\psi + \theta_{1s}\sin\psi + \theta_{3c}\cos 3\psi + \theta_{3s}\sin 3\psi \\ &+ \theta_{4c}\cos 4\psi + \theta_{4s}\sin 4\psi + \theta_{5c}\cos 5\psi + \theta_{5s}\sin 5\psi \end{aligned} \tag{3}$$

where $\psi_i = \psi + 2\pi i/N$, $i = 0, \ldots, N-1$ is the azimuth angle, and the number of blades $N = 4$. Therefore, the input harmonics are defined in the rotating system, but they are identical for each blade. This arrangement will be defined as HHC, although it could also fall under some definitions of IBC. Note that the HHC inputs are assumed to be applied through active pitch links, and using acceleration sensors in the fixed system (hub or fuselage), however, the theoretical development that follows is essentially independent of the specific configuration for actuators and sensors.

The vector $\mathbf{u}_{\mathrm{FCS}}(t)$ contains the controls that would be applied by the pilot or the flight control system. For the derivations of the paper $\mathbf{u}_{\mathrm{FCS}}(t)$ is defined as

$$\mathbf{u}_{\mathrm{FCS}}(t) = [\theta_0(t) \;\; \theta_{1c}(t) \;\; \theta_{1s}(t)]^T \tag{4}$$

The input vector $\mathbf{u}_{\mathrm{FCS}}(t)$ actually used in the simulations also includes the tail rotor collective pitch $\theta_t(t)$. The partition $\mathbf{u}_{\mathrm{HHC}}(t)$ contains the harmonics of the HHC system, that is

$$\mathbf{u}_{\mathrm{HHC}}(t) = [\theta_{3c}(t) \;\; \theta_{3s}(t) \;\; \theta_{4c}(t) \;\; \theta_{4s}(t) \;\; \theta_{5c}(t) \;\; \theta_{5s}(t)]^T \tag{5}$$

The development that follows only addresses the HHC control loops. In fact, the primary meaning of the words "closed loop" is that the HHC vibration control loops are closed. Although small amounts of pitch and roll attitude and rate feedback were added to stabilize the flight dynamic modes, such a simple flight control system architecture is not realistic enough to allow reliable studies of HHC-flight control system interaction. The HHC analysis holds, under linearity assumptions, regardless of whether the FCS loops are open or closed. This is not necessarily true for the effects on the full nonlinear dynamics of the helicopter.

The output vector $\mathbf{y}_H(t)$ can be formed with any of the three linear and three angular components of the accelerations, measured at one or more points of the airframe [the dimensions of $\mathbf{u}(t)$ and $\mathbf{y}(t)$ need not be the same]. The output matrices $C_H(t)$, $D_{\mathrm{FCS}}(t)$, and $D_{\mathrm{HHC}}(t)$ in Eq. (1) therefore depend on the specific form of the output vector $\mathbf{y}_H(t)$ (i.e., on the specific arrangement of sensors), and will be provided later in the paper.

Higher Harmonic Control

The HHC controller used in the present study is based on a linear, steady-state, frequency domain representation of the dynamics of the helicopter. The vector $\tilde{\mathbf{u}}_{\mathrm{HHC}}(k)$ of the harmonics of the rotor controls computed by the HHC system is defined as

$$\tilde{\mathbf{u}}_{\mathrm{HHC}}(k) = [\theta_{3c}(k) \;\; \theta_{3s}(k) \;\; \theta_{4c}(k) \;\; \theta_{4s}(k) \;\; \theta_{5c}(k) \;\; \theta_{5s}(k)]^T \tag{6}$$

where k is the discrete-time index associated with the sample time at which the control loop operates (1/rev). The vector $\tilde{\mathbf{y}}_{\mathrm{HHC}}(k)$ contains the N/rev cosine and sine harmonics of the fuselage accelerations, and is defined as

$$\begin{aligned} &\tilde{\mathbf{y}}_{\mathrm{HHC}}(k) \\ &\quad = [\tilde{y}^1_{Nc}(k) \;\; \tilde{y}^2_{Nc}(k) \;\; \cdots \;\; \tilde{y}^n_{Nc}(k) \;\; \tilde{y}^1_{Ns}(k) \;\; \tilde{y}^2_{Ns}(k) \;\; \cdots \;\; \tilde{y}^n_{Ns}(k)]^T \end{aligned} \tag{7}$$

where $\tilde{y}^i_{Nc}(k)$ and $\tilde{y}^i_{Ns}(k)$, $i = 1, \ldots, n$ are, respectively, the cosine and sine components of the ith N/rev output $\tilde{y}^i(k)$, each defined as

$$\tilde{y}^{\,i}_{Nc}(k) = \frac{1}{\pi}\int_{k\pi}^{(k+1)\pi} y^i_H(\psi)\cos N\psi \,\mathrm{d}\psi \tag{8}$$

$$\tilde{y}^{\,i}_{Ns}(k) = \frac{1}{\pi}\int_{k\pi}^{(k+1)\pi} y^i_H(\psi)\sin N\psi \,\mathrm{d}\psi \tag{9}$$

The generic output $\tilde{y}^i(k)$ can be one of the linear or angular components of the accelerations, which in turn can be measured at one or more locations. In general, there will be n such measurements, and therefore the measurement vector will have $p = 2n$ elements. Finally, $\tilde{\mathbf{y}}^o$ is the vector of N/rev disturbance components corresponding to $\tilde{\mathbf{y}}_{\mathrm{HHC}}(k)$.

Then, assuming that the accelerations are linearly related to the HHC harmonics, the variables defined above can be related by

$$\tilde{\mathbf{y}}_{\mathrm{HHC}}(k) = T_C\tilde{\mathbf{u}}_{\mathrm{HHC}}(k) + \tilde{\mathbf{y}}^o(k) \tag{10}$$

where T_C is a real, constant-coefficient matrix that links the harmonics of the HHC inputs to those of the acceleration response (see [8] for details). The matrix T_C can be either estimated from measured data using online or offline identification algorithms, or computed on the basis of a mathematical model of the helicopter, as done in the present study. In general, T_C is a function of the flight condition. At each discrete-time step the HHC controller selects the value of the input harmonics $\tilde{\mathbf{u}}_{\mathrm{HHC}}$ to reduce the effect of $\tilde{\mathbf{y}}^o$ on $\tilde{\mathbf{y}}_{\mathrm{HHC}}$. Assuming that the baseline acceleration vector $\tilde{\mathbf{y}}^o$ is constant over the time step, the optimal open-loop solution is given by

$$\tilde{\mathbf{u}}_{\mathrm{HHC}}(k) = -T_C^{\dagger}\tilde{\mathbf{y}}^o(k) \tag{11}$$

where $T_C^{\dagger}$ is the pseudoinverse of the T_C matrix (which is not necessarily square). Because, in general, $\tilde{\mathbf{y}}^o$ cannot be measured directly, the same result can be obtained by using a discrete-time integral control law in closed loop, that is, based on the measurements of $\tilde{\mathbf{y}}_{\mathrm{HHC}}$:

$$\tilde{\mathbf{u}}_{\mathrm{HHC}}(k+1) = \tilde{\mathbf{u}}_{\mathrm{HHC}}(k) - T_C^{\dagger}\tilde{\mathbf{y}}_{\mathrm{HHC}}(k) \tag{12}$$

The HHC control algorithm used in the present study is defined in terms of the minimization of a quadratic cost function J of the form [16]

$$J = \tilde{\mathbf{y}}_{\mathrm{HHC}}^T W \tilde{\mathbf{y}}_{\mathrm{HHC}} + \Delta\tilde{\mathbf{u}}_{\mathrm{HHC}}^T R \Delta\tilde{\mathbf{u}}_{\mathrm{HHC}} \tag{13}$$

where $W = W^T \geq 0$ and $R = R^T > 0$ are matrices that allow different weighting of acceleration outputs and $\Delta\tilde{\mathbf{u}}_{\mathrm{HHC}}$ is the increment of $\tilde{\mathbf{u}}_{\mathrm{HHC}}$ from one iteration to the next:

$$\Delta\tilde{\mathbf{u}}_{\mathrm{HHC}}(k+1) = \tilde{\mathbf{u}}_{\mathrm{HHC}}(k+1) - \tilde{\mathbf{u}}_{\mathrm{HHC}}(k) \tag{14}$$

The minimization of J, Eq. (13) leads to the control law

$$\Delta\tilde{\mathbf{u}}_{\mathrm{HHC}}(k+1) = -\left(T_C^T W T_C + R\right)^{-1} T_C^T W \tilde{\mathbf{y}}_{\mathrm{HHC}}(k) \tag{15}$$

The T_C matrix links the N/rev harmonics of the output to the harmonics of the HHC input vector $\tilde{\mathbf{u}}_{\mathrm{HHC}}$. The matrix is fixed and is obtained from the linearized model of the complete helicopter using a methodology based on the harmonic transfer function. The derivation is presented in detail in [8].

Architecture of the HHC System

The present study focuses on the simulation of the HHC architecture shown in general form in Fig. 1. The operation of the system consists of the following three steps, which are performed at every rotor revolution: 1) the determination of the N/rev acceleration output vector $\tilde{\mathbf{y}}_{\mathrm{HHC}}(k)$; 2) the update $\tilde{\mathbf{u}}_{\mathrm{HHC}}(k+1)$ of the control input using Eq. (15); and 3) the actual application of $\tilde{\mathbf{u}}_{\mathrm{HHC}}(k+1)$ via a simple zero-order hold.

Two different sampling rates are used. The first, and faster, corresponds to the sampling of the acceleration signals required to reconstruct the N/rev harmonics. The second, and slower, is that corresponding to the $1/\mathrm{rev}$ update of the HHC inputs. The portions of the block diagram where each sampling rate is used are shown in Fig. 1.

The closed-loop analysis of the helicopter with the HHC system is carried out as follows:

1) discrete-time models are obtained for each of the components of the control loop, including the block representing the dynamics of the helicopter;

2) a complete model is obtained for the series connection of hold circuit, helicopter, and harmonic analyzer: this model will prove to be time periodic;

3) a time-invariant reformulation of the complete model is obtained using the theory of time lifting of periodic systems, using the slower sampling rate (i.e., that of the controller);

4) the overall closed-loop stability analysis is carried out in discrete time.

Discrete Models of the Loop Components

In this section, discrete-time models of all the elements in the closed-loop scheme of Fig. 1 are derived. They include the following: 1) the helicopter model, 2) the harmonic analyzer, 3) the controller, and 4) the zero-order hold.

According to the architecture defined in the previous section, the HHC inputs are updated at $1/\mathrm{rev}$, while the outputs are sampled at a higher frequency to allow the reconstruction of the N/rev component of the accelerations of interest.

Discrete Helicopter Model

The discrete-time helicopter dynamic model is obtained from the linearized continuous-time model of Eq. (1). The sampling frequency is the faster of the two in the system, that is, that required to allow the reconstruction of the N/rev component of the accelerations of interest.

Writing the state and output equations (1) for the helicopter model over a sampling interval P, under the usual assumption of constant input in the interval, one can write the analytical solution for the continuous state vector $\mathbf{x}_H(t)$ at time $t = \eta P + P$ as

$$\mathbf{x}_H(\eta P + P) = \Phi_H(\eta P + P, \eta P)\mathbf{x}_H(\eta P) + \int_{\eta P}^{\eta P + P} \Phi_H(\eta P + P, \tau) B_H(\tau) \mathbf{u}_{\mathrm{HHC}}(\tau)\, \mathrm{d}\tau \tag{16}$$

$$\mathbf{y}_H(\eta P) = C_H(\eta P)\mathbf{x}_H(\eta P) + D_H(\eta P)\mathbf{u}_{\mathrm{HHC}}(\eta P) \tag{17}$$

where Φ_H is the state transition matrix associated with the state matrix A_H. Defining the discrete-time state vector $\tilde{\mathbf{x}}_H$ as $\tilde{\mathbf{x}}_H(\eta) = \mathbf{x}_H(\eta P)$ (similarly for the control vector $\mathbf{u}_{\mathrm{HHC}}$ and the output vector $\mathbf{y}_H$) results in the following discrete-time, state-space linearized model of the helicopter:

$$\begin{aligned} \tilde{\mathbf{x}}_H(\eta + 1) &= \tilde{A}_H(\eta)\tilde{\mathbf{x}}_H(\eta) + \tilde{B}_H(\eta)\tilde{\mathbf{u}}_{\mathrm{HHC}}(\eta) \\ \tilde{\mathbf{y}}_H(\eta) &= \tilde{C}_H(\eta)\tilde{\mathbf{x}}_H(\eta) + \tilde{D}_H(\eta)\tilde{\mathbf{u}}_{\mathrm{HHC}}(\eta) \end{aligned} \tag{18}$$

where the system matrices are defined as

$$\tilde{A}_H(\eta) = \Phi_H(\eta P + P, \eta P) \tag{19}$$

$$\tilde{B}_H(\eta) = \int_0^P \Phi_H(\eta P + P, \tau' + \eta P) B_H(\tau' + \eta P)\, \mathrm{d}\tau' \tag{20}$$

$$\tilde{C}_H(\eta) = C_H(\eta P) \tag{21}$$

$$\tilde{D}_H(\eta) = D_H(\eta P) \tag{22}$$

The system matrices are periodic, with a common period equal to n_s samples. The vector $\tilde{\mathbf{y}}_H(\eta)$ is the vector y in Fig. 1.

Harmonic Analysis

To implement the HHC control algorithm, the N/rev components $\tilde{\mathbf{y}}_{\mathrm{HHC}}$ of the output accelerations must be extracted from their time domain measurements $\tilde{\mathbf{y}}_H$. In each period, the information about $\mathbf{y}_H$ is available starting from $\eta = n_s/2 - 1 + Kn_s$, $K = 1, 2, \ldots$, but is provided as output only at $\eta = (K+1)n_s$. The operation of the harmonic analyzer can be described mathematically by a linear time-periodic (LTP) model with discrete time η and period n_s:

$$\begin{aligned} \tilde{\mathbf{x}}_F(\eta + 1) &= \tilde{A}_F(\eta)\tilde{\mathbf{x}}_F(\eta) + \tilde{B}_F(\eta)\tilde{\mathbf{y}}_H(\eta) \\ \tilde{\mathbf{y}}_{\mathrm{HHC}}(\eta) &= \tilde{C}_F(\eta)\tilde{\mathbf{x}}_F(\eta) \end{aligned} \tag{23}$$

The matrices $\tilde{A}_F(\eta)$, $\tilde{B}_F(\eta)$, and $\tilde{C}_F(\eta)$ are defined in a way that reflects the various phases of the harmonic analysis that occur over one rotor revolution. The vector $\tilde{\mathbf{y}}_{\mathrm{HHC}}(\eta)$ is the vector Y in Fig. 1. For the four-bladed rotor of this study there are three distinct phases, defined as follows (see also Fig. 2):

1) *During the first quarter of the period*, $\eta = 1, 2, \ldots, n_s/4$, the output signal $\mathbf{y}_H$ is allowed to reach steady state following the update of the control input $\mathbf{u}_{\mathrm{HHC}}$ at the end of the previous rotor revolution.

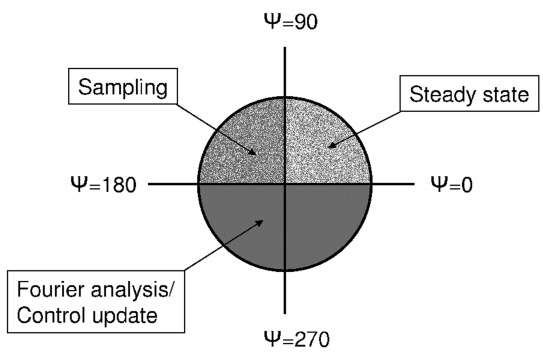

Fig. 2 Operation of the control system over one rotor revolution period T, as a function of the azimuth angle ψ.

During this time, the output of the harmonic analyzer is set to zero and the vectors $\mathbf{y}_H$ measured are not accumulated in the integrals, Eqs. (8) and (9). Therefore the state-space matrices of the harmonic analyzer are given by

$$\tilde{A}_F(\eta) = I \qquad \tilde{B}_F(\eta) = 0 \qquad \tilde{C}_F(\eta) = 0 \tag{24}$$

2) *During the second quarter of the period*, $\eta = n_s/4 + 1, n_s/4 + 2, \ldots, n_s/2$, the outputs $\mathbf{y}_H$ are actually sampled and the integrals, Eqs. (8) and (9), computed, but the output of the analyzer is still kept to zero. Note that the state of the harmonic analyzer must be reset to zero at the beginning of the second quarter of the period, so the state-space matrices will be defined as

$$\tilde{A}_F(\eta) = \begin{cases} 0 & \eta = \frac{n_s}{4} \\ I & \text{elsewhere} \end{cases} \tag{25}$$

$$\tilde{B}_F(\eta) = \text{blkdiag}\left\{ \begin{bmatrix} \sin\left(\frac{2N\pi}{n_s}\eta\right) \\ \cos\left(\frac{2N\pi}{n_s}\eta\right) \end{bmatrix} \right\} \tag{26}$$

$$\tilde{C}_F(\eta) = 0 \tag{27}$$

3) *During the remaining half period*, $\eta = n_s/2 + 1, n_s/2 + 2, \ldots, n_s$, the new value of the control input $\tilde{\mathbf{u}}_{\text{HHC}}$ is computed and applied to the rotor; therefore the operation of the analyzer is stopped and the computed value for the N/rev harmonic of $\mathbf{y}_H$ is made available at the end of the period:

$$\tilde{A}_F(\eta) = I \tag{28}$$

$$\tilde{B}_F(\eta) = 0 \tag{29}$$

$$\tilde{C}_F(\eta) = \begin{cases} \frac{8}{n_s} I & \eta = n_s \\ 0 & \text{elsewhere} \end{cases} \tag{30}$$

The entire sequence of operations described above can be summarized in the following expressions for the state-space matrices of the harmonic analyzer, which hold for a generic value of the 1/rev discrete-time index k (i.e., for the generic, kth rotor revolution):

$$\tilde{A}_F(\eta) = \begin{cases} 0 & \eta = kn_s + \frac{n_s}{4} \\ I & \text{elsewhere} \end{cases} \tag{31}$$

$$\beta_F(\eta) = \begin{cases} 1 & kn_s + \frac{n_s}{4} \le \eta < kn_s + \frac{n_s}{2} \\ 0 & \text{elsewhere} \end{cases} \tag{32}$$

$$\tilde{B}_F(\eta) = \beta_F(\eta)\text{blkdiag}\left\{ \begin{bmatrix} \sin\left(\frac{2N\pi}{n_s}\eta\right) \\ \cos\left(\frac{2N\pi}{n_s}\eta\right) \end{bmatrix} \right\} \tag{33}$$

$$\tilde{C}_F(\eta) = \begin{cases} \frac{8}{n_s} I & \eta = kn_s + n_s \\ 0 & \text{elsewhere} \end{cases} \tag{34}$$

Therefore, the output of the above model is nonzero only for $\eta = 0, n_s, 2n_s, \ldots$.

Controller

The control law given by Eq. (15) can be written in state-space form as a linear time-invariant system

$$\tilde{\mathbf{x}}_C(k+1) = \tilde{A}_C\tilde{\mathbf{x}}_C(k) + \tilde{B}_C\tilde{\mathbf{y}}_{\text{HHC}}(k) \tag{35}$$

$$\tilde{\mathbf{u}}_{\text{HHC}}(k) = \tilde{C}_C\tilde{\mathbf{x}}_C(k) \tag{36}$$

where

$$\tilde{A}_C = I \tag{37}$$

$$\tilde{B}_C = -\left\{T_C^T W T_C + R\right\}^{-1} T_C^T W \tag{38}$$

$$\tilde{C}_C = I \tag{39}$$

The vector $\tilde{\mathbf{u}}_{\text{HHC}}(k)$ is the vector U in Fig. 1.

Zero-Order-Hold Circuit

The hold circuit is the interface between the controller and the helicopter. Because the controller operates at the discrete-time k (i.e., once per revolution) while the helicopter model has been obtained at the discrete-time η (i.e., once per sample needed to extract the N/rev harmonics), the controller provides a new value of the control variables only at $\eta = kn_s$, $k = 1, 2, \ldots$, and this output must be kept constant for the intervening samples $kn_s \le \eta < (k+1)n_s$. Therefore, the model of the hold circuit is linear, discrete-time periodic, with discrete-time η and period n_s, and is given by

$$\tilde{\mathbf{x}}_Z(\eta+1) = \tilde{A}_Z(\eta)\tilde{\mathbf{x}}_Z(\eta) + \tilde{B}_Z(\eta)\tilde{\mathbf{u}}_{\text{HHC}}(\eta) \tag{40}$$

$$\mathbf{u}_{\text{HHC}}(\eta) = \tilde{C}_Z(\eta)\tilde{\mathbf{x}}_Z(\eta) + \tilde{D}_Z(\eta)\tilde{\mathbf{u}}_{\text{HHC}}(\eta) \tag{41}$$

where

$$\tilde{A}_Z(\eta) = \delta(\eta) \tag{42}$$

$$\tilde{B}_Z(\eta) = I - \delta(\eta) \tag{43}$$

$$\tilde{C}_Z(\eta) = \delta(\eta) \tag{44}$$

$$\tilde{D}_Z(\eta) = I - \delta(\eta) \tag{45}$$

and

$$\delta(\eta) = \begin{cases} 0 & \eta = kn_s, k = 1, 2, \ldots \\ I & \text{elsewhere} \end{cases} \tag{46}$$

The vector $\tilde{\mathbf{u}}_{\text{HHC}}(\eta)$ is the vector U in Fig. 1.

Series Connection of Zero-Order-Hold, Helicopter Model and Harmonic Analyzer

The overall discrete HHC model, which relates the harmonics of the HHC input $\tilde{\mathbf{u}}_{\text{HHC}}$ to the harmonics of the acceleration output $\tilde{\mathbf{y}}_{\text{HHC}}$ can be obtained by connecting in series the harmonic analyzer, Eq. (23), the discrete model for the response of the helicopter to HHC inputs, Eq. (16), and that of the zero-order-hold, Eq. (40). The model, with discrete-time η, is given by

$$\tilde{\mathbf{x}}_Z(\eta+1) = \tilde{A}_Z\tilde{\mathbf{x}}_Z(\eta) + \tilde{B}_Z\tilde{\mathbf{u}}_{\text{HHC}}(\eta) \tag{47}$$

$$\tilde{\mathbf{x}}_H(\eta+1) = \tilde{A}_H\tilde{\mathbf{x}}_H(\eta) + \tilde{B}_H\tilde{C}_Z\tilde{\mathbf{x}}_Z(\eta) + \tilde{B}_H\tilde{D}_Z\tilde{\mathbf{u}}_{\text{HHC}}(\eta) \tag{48}$$

$$\tilde{\mathbf{x}}_F(\eta+1) = \tilde{A}_F\tilde{\mathbf{x}}_F(\eta) + \tilde{B}_F\tilde{C}_H\tilde{\mathbf{x}}_H(\eta) + \tilde{B}_F\tilde{D}_H\tilde{C}_Z\tilde{\mathbf{x}}_Z(\eta) + \tilde{B}_F\tilde{D}_H\tilde{D}_Z\tilde{\mathbf{u}}_{\text{HHC}}(\eta) \tag{49}$$

$$\tilde{\mathbf{y}}_{\text{HHC}}(\eta) = \tilde{C}_F \tilde{\mathbf{x}}_F(\eta) \tag{50}$$

(the argument η in the matrices has been omitted for simplicity). This model cannot be connected directly to the HHC controller because its sampling rate is still different from that of the discrete HHC control law (n_s/rev vs 1/rev). A combined model at the same sampling rate as the HHC controller can be obtained using the theory of time-invariant reformulations of linear time-periodic systems and, more precisely, through a time-lifted reformulation.

Time-Lifted Formulation of the Closed-Loop System

A closed-loop stability analysis requires a single sampling period for the entire system. Therefore, the model will be reformulated using the shorter sampling period $P = T/n_S$ as the common period. The implicit assumption that the longer sampling period T, corresponding to one rotor revolution, is an integer multiple of the acceleration sampling period P is clearly quite reasonable. This reformulation is carried out using time lifting, and results in a discrete model with overall sampling period T and time index k. Time lifting is described in detail in [17] and is summarized in [18], which also contains numerical examples of the application to a flapping rigid rotor blade. A useful byproduct of the use of a lifted reformulation is that the resulting model has constant coefficients, which simplifies the closed-loop stability analysis.

Time Lifting of Periodic Systems

Time lifting is based on the idea that the knowledge of the state vector at time k and of the inputs between time k and $k+1$ is sufficient to determine the value of the state at time $k+1$ and the value of the outputs between k and $k+1$. The key steps of time lifting will be briefly outlined here.

Consider the linear, discrete-time periodic system with a period equal to n_s samples, and with m inputs and p outputs

$$\tilde{\mathbf{x}}(t+1) = A(t)\tilde{\mathbf{x}}(t) + B(t)\tilde{\mathbf{u}}(t) \qquad \tilde{\mathbf{y}}(t) = C(t)\tilde{\mathbf{x}}(t) + D(t)\tilde{\mathbf{u}}(t) \tag{51}$$

where $t = 0, 1, 2, \ldots, n_s - 1$. Then, the state vector at time $t > \tau$ is given by the discrete-time Lagrange formula [19]

$$\tilde{\mathbf{x}}(t) = \Psi(t,\tau)\tilde{\mathbf{x}}(\tau) + \sum_{j=\tau+1}^{t} \Psi(t,j)B(j-1)\tilde{\mathbf{u}}(j-1) \tag{52}$$

where $\Psi(t,\tau) = A(t-1)A(t-2)\cdots A(\tau)$ is the transition matrix from time τ (also an integer between 0 and $n_s - 1$) to time t for the state equation (51). Equation (52) can be used to build an equivalent (i.e., with the same output given the same input) time-invariant system by sampling the state vector at a frequency of n_s, and packing the input and output vectors for each sample into larger input and output vectors. This results in the "lifted" reformulation [17,18]

$$\tilde{\mathbf{x}}(k+1) = F\tilde{\mathbf{x}}(k) + G\mathbf{u}_{\text{lift}}(k) \qquad \mathbf{y}_{\text{lift}}(k) = H\tilde{\mathbf{x}}(k) + E\mathbf{u}_{\text{lift}}(k) \tag{53}$$

where the extended input vector $u_{\text{lift}}(k)$ has size mn_s and is defined as

$$\mathbf{u}_{\text{lift}}(k) = [\tilde{\mathbf{u}}(kn_s)^T \quad \cdots \quad \tilde{\mathbf{u}}(kn_s + n_s - 1)^T]^T$$

and the extended output vector $\mathbf{y}_{\text{lift}}(k)$ has size pn_s and is defined as

$$\mathbf{y}_{\text{lift}}(k) = [\tilde{\mathbf{y}}(kn_s)^T \quad \cdots \quad \tilde{\mathbf{y}}(kn_s + n_s - 1)^T]^T$$

The time-invariant system matrices F, G, H, and E have dimensions, respectively, of n by n, n by mn_s, pn_s by n, and pn_s by mn_s and are given by [17,18]

$$F = A(n_s - 1)A(n_s - 2)\cdots A(0) \tag{54}$$

$$G = [\Psi(n_s,1)B(0) \quad \Psi(n_s,2)B(1) \quad \cdots \quad \Psi(n_s,n_s)B(n_s-1)] \tag{55}$$

$$H = [C(0)^T \quad \Psi(1,0)^T C(1)^T \quad \cdots \quad \Psi(n_s-1,0)^T C(n_s-1)^T]^T \tag{56}$$

$$E = \{(E_{ij})\}, \qquad i,j = 1,2,\ldots n_s \tag{57}$$

with

$$E_{ij} = \begin{cases} 0 & i < j \\ D(i-1) & i = j \\ C(i-1)\Psi(i-1,j)B(j-1) & i > j \end{cases} \tag{58}$$

It should be noted that the matrix F is the Floquet transition matrix of the discrete-time periodic system (51); therefore the constant-coefficient lifted system of Eq. (53) has exactly the same stability characteristics as the time-periodic system. This Floquet transition matrix is also the same as that of the original continuous system, and therefore continuous and discrete systems also have the same stability characteristics [17,18].

Lifted Form of the HHC Loop

Time lifting can be directly applied to the coupled helicopter/HHC system, Eqs. (47–50). The corresponding lifted form is given by

$$\tilde{\mathbf{x}}(k+1) = F\tilde{\mathbf{x}}(k) + G\mathbf{u}_{\text{lift}}(k) \tag{59}$$

$$\mathbf{y}_{\text{lift}}(k) = H\tilde{\mathbf{x}}(k) + E\mathbf{u}_{\text{lift}}(k) \tag{60}$$

The input vector $\mathbf{u}_{\text{lift}}(k)$ is given by

$$\mathbf{u}_{\text{lift}}(k) = \begin{bmatrix} I \\ I \\ \vdots \\ I \end{bmatrix} \tilde{\mathbf{u}}_{\text{HHC}}(k) \tag{61}$$

where the mn_s by m matrix that relates $\mathbf{u}_{\text{lift}}(k)$ and $\tilde{\mathbf{u}}_{\text{HHC}}(k)$ is obtained by assembling n_s identity matrices because the HHC input vector $\tilde{\mathbf{u}}_{\text{HHC}}(k)$ is held constant over all the n_s samples that make up one rotor revolution.

Similarly, once the lifted output vector $\mathbf{y}_{\text{lift}}$ has been obtained as the output of the lifted system, Eqs. (59) and (60), the actual discrete output vector $\tilde{\mathbf{y}}_{\text{HHC}}(k)$ can be recovered by observing that it is the output of the Fourier coefficients extractor, which is only evaluated once per revolution, that is, at times $\eta = 0, n_s, 2n_s, \ldots$. Therefore

$$\tilde{\mathbf{y}}_{\text{HHC}}(k) = [I \;\; 0]\mathbf{y}_{\text{lift}}(k) \tag{62}$$

where $\mathbf{y}_{\text{HHC}}(k)$ has size p and $\mathbf{y}_{\text{lift}}(k)$ has size pn_s. On the basis of Eqs. (61) and (62), and recalling the state-space form for the discrete HHC controller, Eqs. (35) and (36), the overall closed-loop system can be constructed as follows:

$$\tilde{\mathbf{x}}(k+1) = F\tilde{\mathbf{x}}(k) + G\begin{bmatrix} I \\ I \\ \vdots \\ I \end{bmatrix} \tilde{C}_C \tilde{\mathbf{x}}_C(k) \tag{63}$$

$$\tilde{\mathbf{x}}_C(k+1) = B_C[I \;\; 0]H\tilde{\mathbf{x}}(k) + \left(\tilde{A}_C + [I \;\; 0]E\begin{bmatrix} I \\ I \\ \vdots \\ I \end{bmatrix} \right) \tilde{\mathbf{x}}_C(k) \tag{64}$$

This closed-loop helicopter/HHC system is now linear time invariant, with discrete-time k and state variables $\tilde{x}_Z$, $\tilde{x}_H$, $\tilde{x}_F$, and $\tilde{x}_C$. Therefore, the closed-loop stability analysis can be carried out by checking the eigenvalues of the closed-loop system.

Results

This section presents closed-loop stability and response results for a coupled helicopter-HHC system. The stability results and the linearized time histories are obtained from the linearized, time-lifted model of Eqs. (63) and (64). The closed-loop response results are obtained from the full nonlinear simulation of the coupled helicopter-HHC system.

The helicopter configuration used for the present study is similar to the Eurocopter B0-105, with a thrust coefficient $C_T/\sigma = 0.071$. The BO-105 configuration is fully described in [20]. Five blade modes are used in the modal coordinate transformation, namely, the fundamental flap, lag, and torsion modes along with the second flap and lag modes, with natural frequencies of 1.12/rev, 0.7/rev, 3.2/rev, 3.4/rev, and 4.5/rev, respectively. Because the aerodynamic model consists of a simple linear inflow with quasi-steady aerodynamics, vibratory loads and center of gravity (CG) accelerations, and consequently also HHC inputs, tend to be underestimated. Therefore, their absolute values can be considered representative only in a qualitative sense. However, the overall simulation model is likely reasonable for stability studies, and for a general assessment of the design and closed-loop analysis methodology.

For all the vibratory response results, the helicopter is first trimmed in steady, straight flight at the desired velocity with the HHC system turned off. Then, the nonlinear simulation begins, with the pilot controls held fixed at their trim values and the HHC system turned on at time $t = 0$.

The controller has been implemented in discrete time using a "fast" sampling rate of $n_s = 36$ samples per rotor revolution. The weighting matrices W and R which define the HHC quadratic performance index, Eq. (13), have been chosen to be proportional to the identity matrix, that is, $W = I$ and $R = rI$.

Results are presented for speeds V of 80 and 140 kt. In all the results of this section, the effects of periodic coefficients in the coupled helicopter-HHC model are taken rigorously into account. It should be noted, however, that at $V = 80$ kt, corresponding to an advance ratio $\mu = 0.188$, the periodicity of the baseline helicopter model without the HHC system is not strong, and a constant-coefficient approximation to the helicopter dynamics, based on a multiblade coordinate transformation, would probably be sufficiently accurate. On the other hand, at $V = 140$ kt the advance ratio is $\mu = 0.33$, and the effects of periodic coefficients would likely be significant (the usually accepted limit is about $\mu = 0.30$–0.35).

Results for $V = 80$ kt

Figure 3 shows the closed-loop, vertical acceleration response $\dot{w}$ for three different values of the tuning parameter r, namely, $r = 2 \times 10^4$ (top plot), $r = 5 \times 10^4$ (center plot), and $r = 10^5$ (bottom plot), corresponding to increasing restrictions on the control effort or, equivalently, to decreasing gain. Note that the scales on the vertical axis are different for each plot. For the value $r = 2 \times 10^4$, the response loosely resembles a limit cycle, but the values of the accelerations are of up to $\pm 1g$, and therefore unacceptably high. For this value of r the linearized analysis predicts an instability. For the value $r = 5 \times 10^4$, the response is unstable, but the values of $\dot{w}$ are now considerably smaller, and remain within $\pm 0.04g$ within the first 7 s. The linearized analysis indicates a mild instability. Finally, for $r = 10^5$, the response becomes stable and the HHC is very effective in suppressing $\dot{w}$. This is also predicted by the linearized analysis. The behavior of roll and pitch accelerations is qualitatively very similar to that of $\dot{w}$, and it will not be shown here.

Similar plots were presented in [8] for the same flight condition and helicopter configuration, but with the HHC closed loop modeled as entirely continuous, and the harmonic analysis, the computation delay, and the zero-order hold not modeled at all. For values of the tuning parameter r ranging from 0 to 10^4 the response was stable, and the HHC would effectively suppress vibrations in 10 s or less. Comparing these results with those shown in Fig. 3, it is clear that the allowable gains of the HHC system must be lower because of the reduction in phase margin brought about by the delays in the HHC loop.

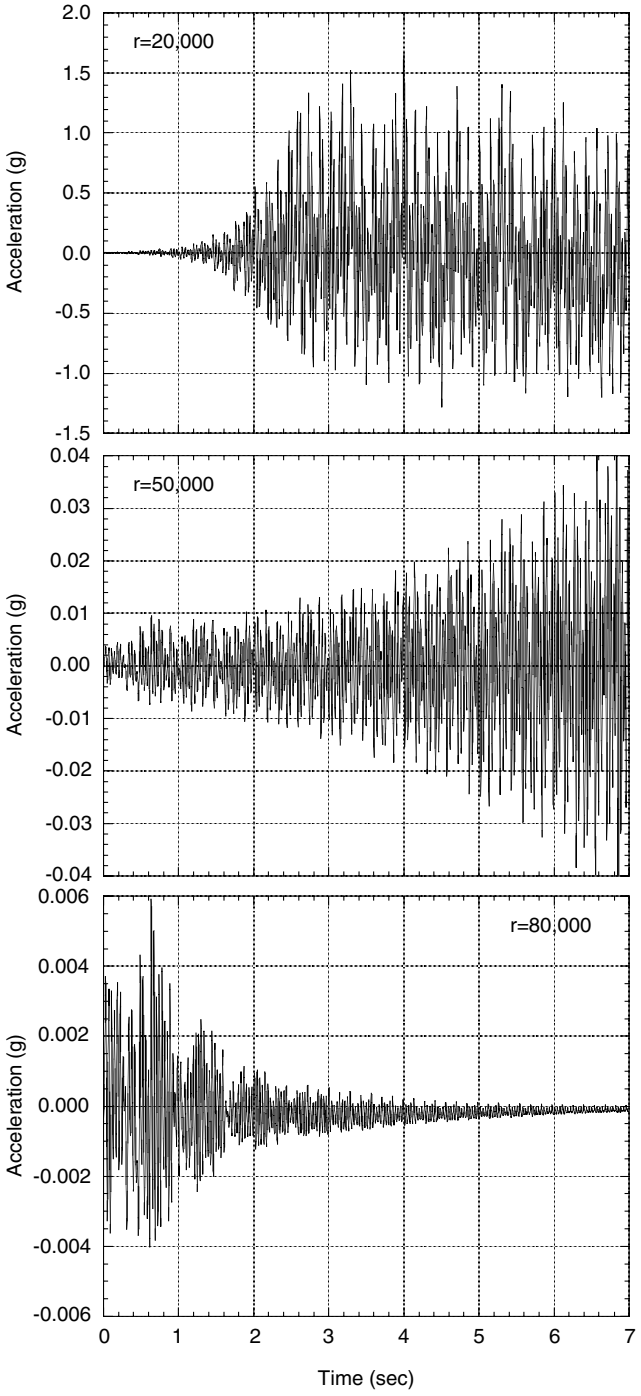

Fig. 3 Vertical accelerations $\dot{w}$ at the helicopter center of mass for $V = 80$ kt ($\mu = 0.188$) and tuning parameter $r = 2 \times 10^4$ (top), $r = 5 \times 10^4$ (center), and $r = 10^5$ (bottom).

Selected closed-loop stability eigenvalues are shown in Fig. 4 as a function of r. The real parts of the eigenvalues are plotted as a function of r. These are the eigenvalues of the discrete system, converted to continuous form. The closed-loop system becomes unstable for $r < 1.5 \times 10^5$. This instability was not captured by the approximate continuous HHC model of [8], which instead predicted closed-loop stability for every value of r. This clearly demonstrates that neglecting the discrete nature of the HHC loop is unconservative, and should be avoided.

Figure 5 shows the time history of the response of just the 4/rev harmonic of $\dot{w}$. The three curves show, respectively, the baseline response with the HHC system turned off, the response predicted by the nonlinear simulation model, and that predicted by the linearized, time-periodic model used to design the HHC system. Apart from a

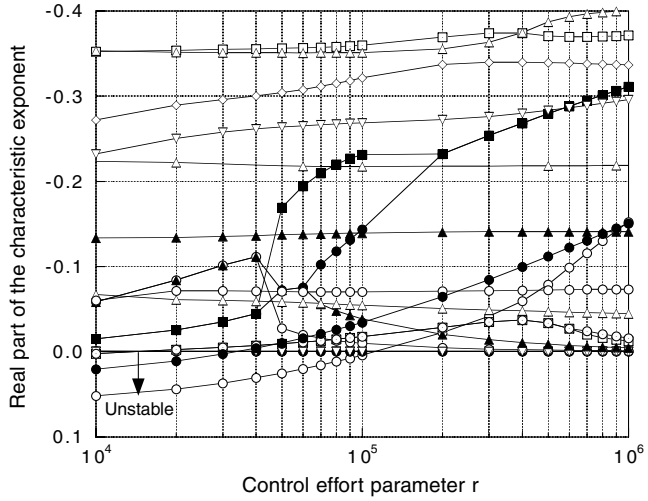

Fig. 4 Real parts of selected closed-loop stability eigenvalues for $V = 80$ kt ($\mu = 0.188$) as a function of the controller tuning parameter r.

small initial transient, caused by a small initial mismatch between the trimmed and the time-marching solution, the baseline 4/rev response rapidly converges to a constant, nonzero steady value. The nonlinear closed-loop response exhibits a brief but strong transient, during which the acceleration increases by almost 3 times the baseline value. The transient lasts for less than 2 s, after which the 4/rev response is rapidly reduced to almost zero. This strong transient is not present in the $\dot{p}$ and $\dot{q}$ 4/rev responses, not shown in the figure, which start being attenuated as soon as the HHC is turned on. The figure also shows that the 4/rev responses predicted by the LTP and by the nonlinear model are nearly identical. This indicates that, for the type of mathematical model used in this study, and for the flight condition considered, 1) the effect of nonlinearities on the 4/rev $\dot{w}$ response is small, and the response is adequately captured by a linearized model as long as the periodicity is retained (the same conclusions hold for $\dot{p}$ and $\dot{q}$), and 2) the LTP model is sufficiently accurate for the HHC design.

The magnitudes of the 3/, 4/, and 5/rev control harmonics are plotted in Fig. 6 as a function of time. The controls for both the rigorous discrete model and the approximate continuous model are shown in the figure. Discrete and continuous controls tend to the same magnitude value, but the initial transients are quite different. The magnitudes of the discrete controls grow much faster than those of the continuous controls. The magnitudes of the 3/ and 4/rev harmonics of the discrete controller reach essentially the respective steady-state values in about 2 s, that of the 5/rev harmonic in about

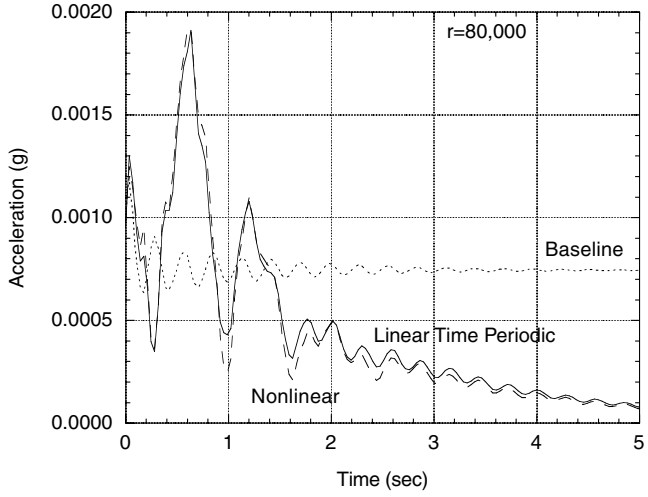

Fig. 5 Closed-loop 4/rev vertical acceleration response $\dot{w}$ at the helicopter center of mass for $V = 80$ kt ($\mu = 0.188$); baseline open-loop response, and prediction with linear and nonlinear simulation models.

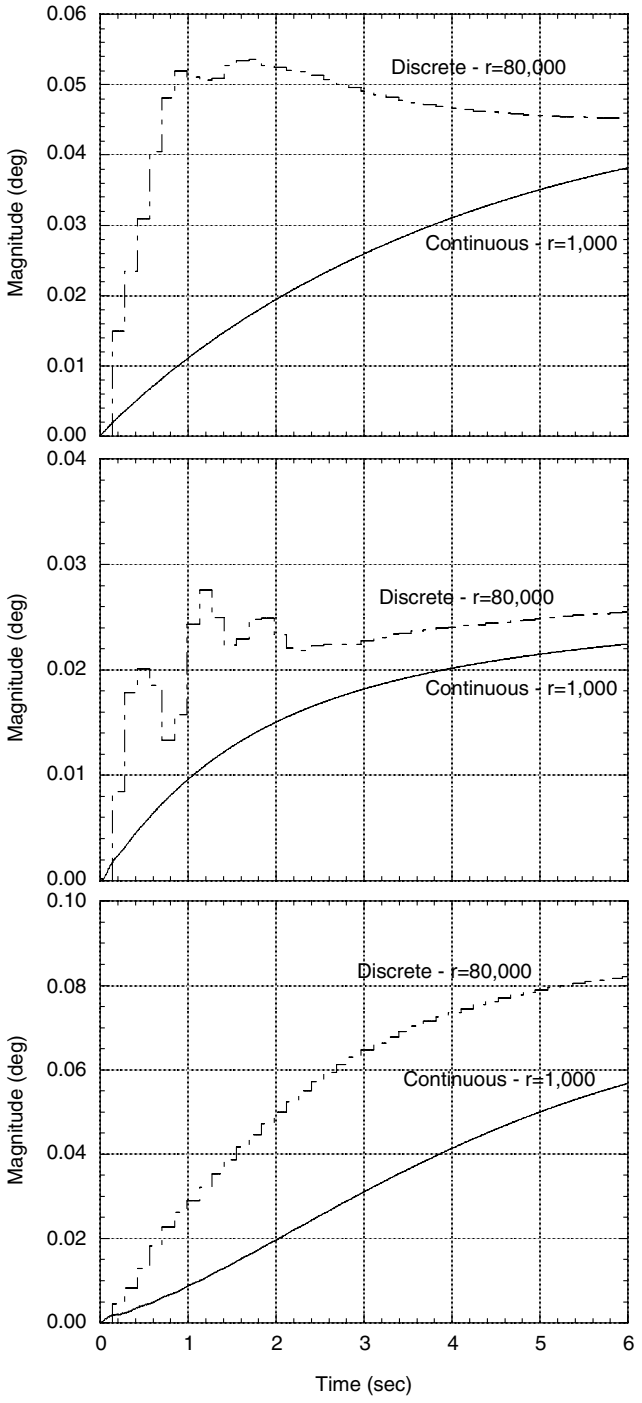

Fig. 6 HHC control input magnitude in degrees for continuous and discrete models, $V = 80$ kt ($\mu \approx 0.189$); 3/rev (top), 4/rev (center), 5/rev (bottom).

6 s. The respective values for the continuous case are well over 6 s for the 3/ and 5/rev, and about 6 s for the 4/rev. This behavior, which is to some extent counterintuitive given that the discrete HHC is operating at a lower gain than the continuous HHC, is responsible for the faster vibration reduction of the discrete HHC.

Better agreement between the phases of the discrete and continuous model can be seen in Fig. 7. Except for the first 1–2 rotor revolutions (slightly more for the 4/rev control), discrete and continuous phases are almost identical.

Results for $V = 140$ kt

Figure 8 shows the closed-loop, vertical acceleration response $\dot{w}$ for three different values of the tuning parameter r, namely, $r = 10^4$ (top plot), $r = 5 \times 10^4$ (center plot), and $r = 10^5$ (bottom plot). The

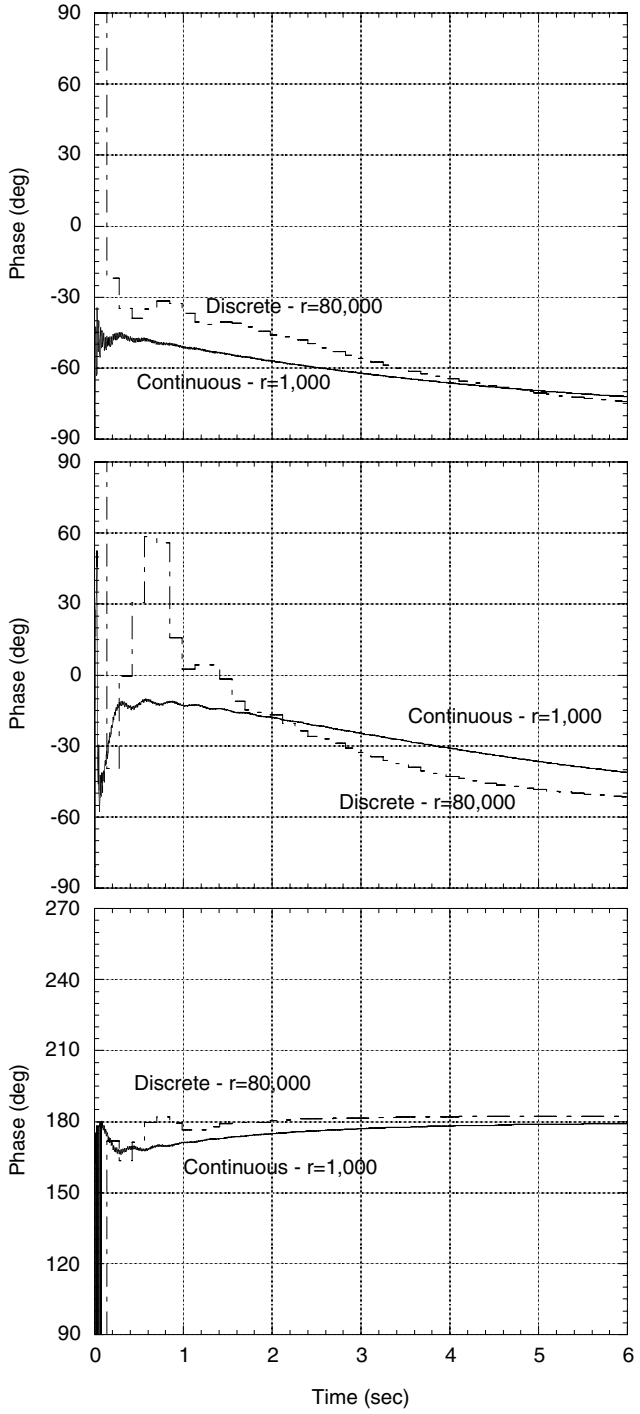

Fig. 7 HHC control input phase in degrees for continuous and discrete models, $V = 80$ kt ($\mu \approx 0.189$); 3/rev (top), 4/rev (center), 5/rev (bottom).

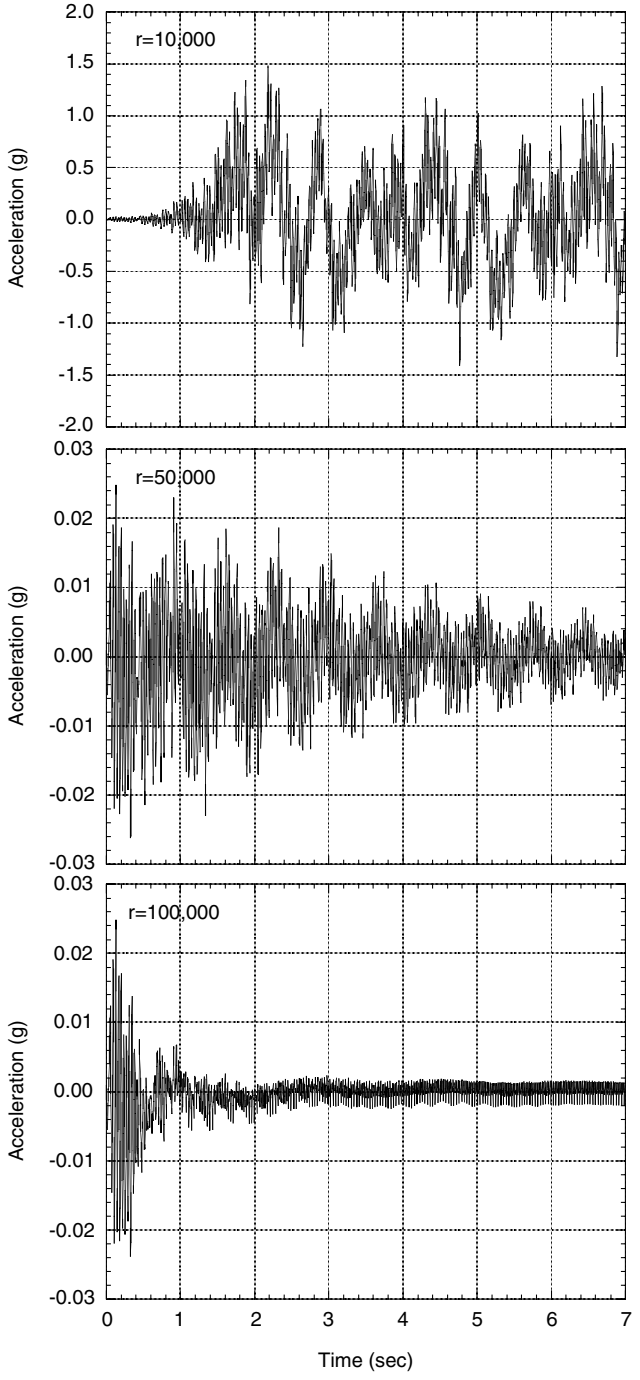

Fig. 8 Vertical accelerations $\dot{w}$ at the helicopter center of mass for $V = 140$ kt ($\mu = 0.330$) and tuning parameter $r = 10^4$ (top), $r = 5 \times 10^4$ (center), and $r = 10^5$ (bottom).

scale on the vertical axis of the top plot is different from those of the other two. As in the 80 kt case, for the value $r = 10^4$ the acceleration response is very high and erratic, with peaks well over $1g$ in absolute value, and loosely resembling a limit cycle. For this value of r the linearized analysis predicts an instability. For the value $r = 5 \times 10^4$ the response is stable, and slowly decreases in magnitude. Finally, for $r = 10^5$, the response is stable and the vibrations are reduced very quickly, in less than 2 s from the application of HHC. The linearized analysis also indicates that these last two cases are stable. The behavior of roll and pitch accelerations is qualitatively very similar to that of $\dot{w}$, and it will not be shown here.

Compared with the corresponding plots of [8], for the same flight condition but with a continuous HHC model, the allowable gains are lower. In [8] the closed-loop system was studied for values of r ranging from 0 to 1000, and in all cases it was stable.

The real parts of selected closed-loop stability eigenvalues for $V = 140$ kt as a function of r are shown in Fig. 9. The closed-loop system at $V = 140$ kt becomes unstable for $r < 1.5 \times 10^5$ in the same fashion that the system at $V = 80$ kt did. Results for $V = 140$ kt are qualitatively very similar to the stability values shown in Fig. 6 for $V = 80$ kt, and the same conclusions on the effects of the discrete nature of the HHC can be reached.

Figure 10 is similar to Fig. 5, but refers to $V = 140$ kt. As in Fig. 5, after a small initial transient, the baseline 4/rev response rapidly converges to a constant, nonzero steady value. The nonlinear closed-loop response no longer exhibits the strong transient observed at $V = 80$ kt, and the 4/rev response is substantially reduced after just

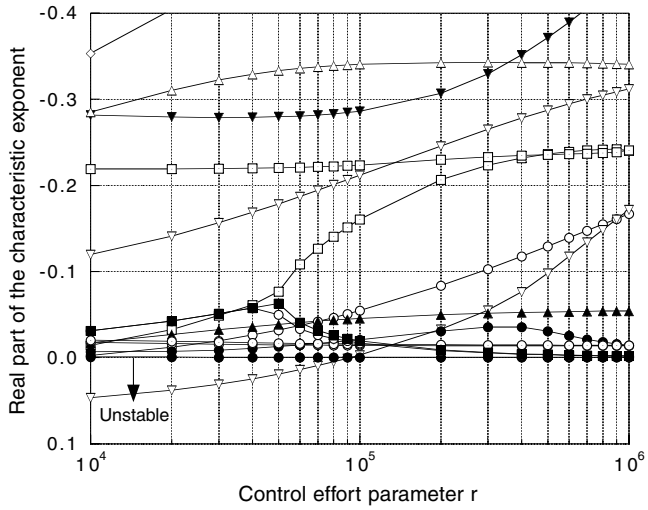

Fig. 9 Real parts of selected closed-loop stability eigenvalues for $V = 140$ kt ($\mu = 0.330$) as a function of the controller tuning parameter r.

1 s. The same happens for the $\dot{p}$ and $\dot{q}$ 4/rev responses, not shown in the figure. As in the $V = 80$ kt case, the 4/rev responses predicted by the LTP and by the nonlinear model are nearly identical, and the same conclusions on the effect of nonlinearities and the adequacy of the LTP model for design purposes apply.

The magnitude of the 3/, 4/, and 5/rev harmonics are plotted in Fig. 11 as a function of time. The controls for both the discrete and the continuous model are shown in the figure. As in the $V = 80$ kt case, discrete and continuous controls tend to the same magnitude value, although the initial transients are quite different and the magnitudes of the discrete controls grow much faster than those of the continuous controls. The magnitudes of all the harmonics of the discrete controller reach their respective steady-state values in about 2 s. The respective values for the continuous case are of 6 s and more.

An almost perfect agreement between the phases of the discrete and continuous model can be seen in Fig. 12. Except for the first few rotor revolutions, discrete and continuous phases are almost identical.

Other Considerations

The results presented in this section underscore the importance of a correct modeling of "real life" effects such as discrete sampling, computations, and control updates, even for the simplified, fixed T-matrix scheme used in this study. Several additional effects were neglected and should be included or more carefully analyzed in

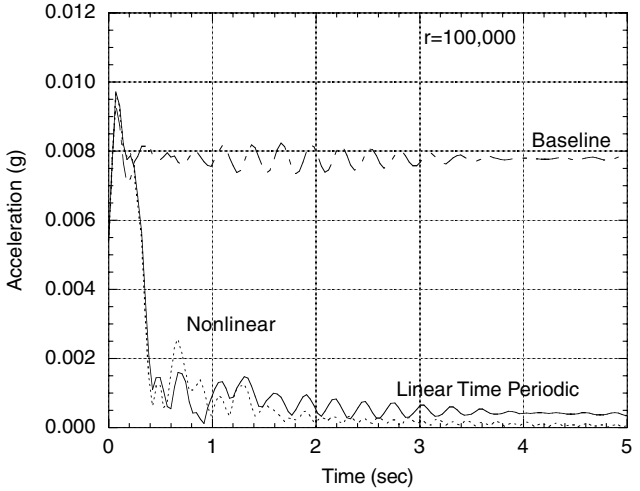

Fig. 10 Closed-loop 4/rev acceleration response $\dot{w}$ at the helicopter center of mass for $V = 140$ kt ($\mu = 0.330$); baseline open-loop response, and prediction with linear and nonlinear simulation model.

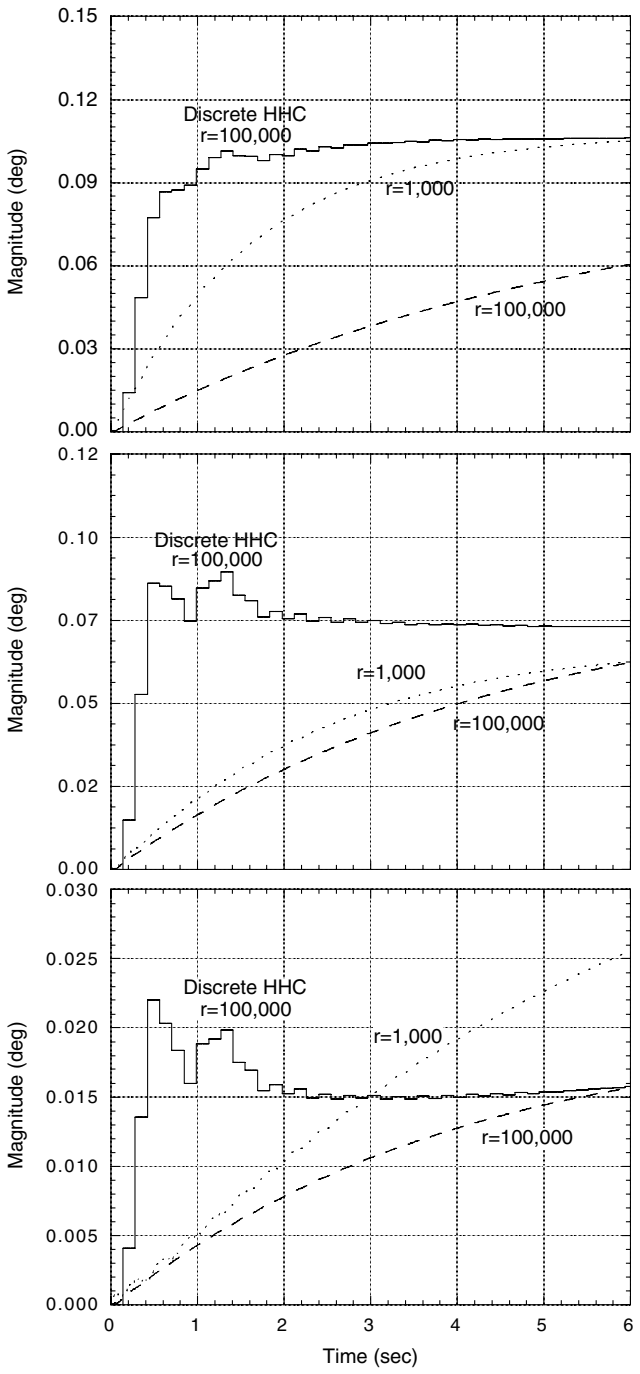

Fig. 11 HHC control input magnitude in degrees for continuous and discrete models, $V = 140$ kt ($\mu = 0.330$); 3/rev (top), 4/rev (center), 5/rev (bottom).

future research. First, in the scheme of Fig. 2, it was assumed that the transient following each HHC update would take one-quarter of a rotor revolution to die out. Simulation results not presented here indicate that a more realistic figure is 1–2 rotor revolutions for well-damped rotors with mechanical lag dampers, and up to 4–6 revolutions for lowly damped hingeless rotors. Second, the HHC update at each rotor revolution was simulated as a pure step. Although rotating system HHC actuators are very fast, they cannot generate such steps, and therefore they add their own delay. Third, perfect measurements were assumed, whereas real sensors introduce their own dynamics in the loop. Fourth, practical digital harmonic analyses will require the use of windows, which may introduce further delays and spurious dynamics. Finally, the most appropriate values of the tuning parameter r will probably be different for each control, rather than identical as in the present study. All these effects

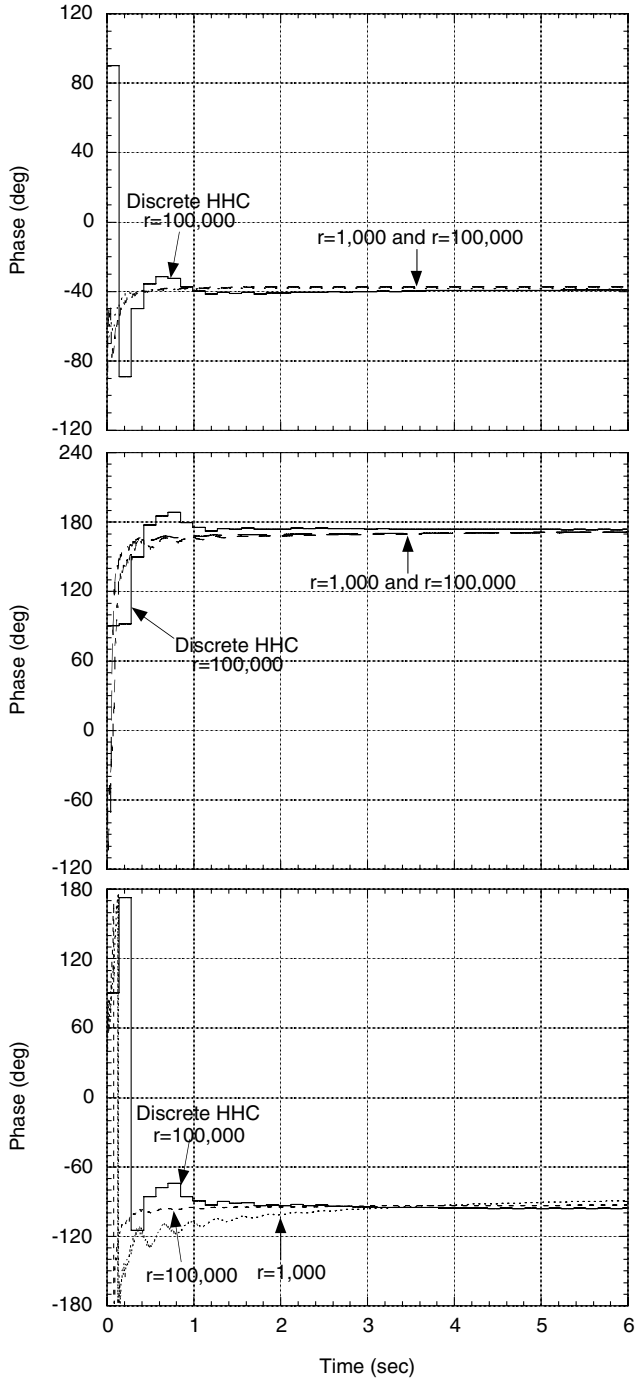

Fig. 12 HHC control input phase in degrees for continuous and discrete models, $V = 140$ kt ($\mu = 0.330$); 3/rev (top), 4/rev (center), 5/rev (bottom).

must be taken into account to obtain realistic predictions of the maximum performance achievable by an HHC system.

Conclusions

This paper presented an aeromechanical closed-loop stability and response analysis of a hingeless rotor helicopter with a higher harmonic control system for vibration reduction. The analysis fully included the rigid body dynamics of the helicopter and the flexibility of the rotor blades. It was assumed that the gain matrix T was fixed and computed offline. The discrete elements of the HHC control loop were rigorously modeled, including the presence of two different time scales in the loop. By also formulating the coupled rotor-fuselage dynamics in discrete form, the entire coupled helicopter-HHC system could be rigorously modeled as a discrete system. Finally, the effect of the periodicity of the equations of motion was rigorously taken into account by converting the system with periodic coefficients into an equivalent system with constant coefficients and identical stability properties using a time-lifting technique.

The most important conclusion of the present study is that the discrete elements in the HHC loop must be modeled in any HHC analysis. Not doing so is unconservative. For the helicopter configuration and HHC structure used in this study, an approximate continuous modeling of the HHC system indicated that the closed-loop, coupled helicopter-HHC system was always stable, whereas the more rigorous discrete analysis shows that closed-loop instabilities can occur. The HHC gains must be reduced to account for the loss of gain margin brought about by the discrete elements.

Other conclusions of the study are 1) the HHC is effective in quickly reducing vibrations, at least at its design condition; 2) a linearized model of helicopter dynamics is adequate for HHC design, as long as the periodicity of the system is correctly taken into account, that is, periodicity is more important than nonlinearity, at least for the mathematical model used in this study; and 3) when discrete and continuous systems are both stable, the predicted HHC control harmonics are in good agreement, although the initial transient behavior can be considerably different.

Acknowledgment

The support of the U.S. Army Research Office, under the project number 41569-EG, "Control of Systems With Periodic Coefficients With Application to Active Rotor Control," Technical Monitor Gary Anderson, is gratefully acknowledged.

References

[1] Welsh, W. A., "Evolution of Active Vibration Control Technology," *Proceedings of the AHS 4th Decennium Specialist's Conference on Aeromechanics*, American Helicopter Society, Alexandria, VA, Jan. 2004.

[2] Johnson, W., "Self-Tuning Regulators for Multicyclic Control of Helicopter Vibration," NASA TP 1996, March 1992.

[3] Friedmann, P. P., and Millott, T. A., "Vibration Reduction in Rotorcraft Using Active Control—A Comparison of Various Approaches," *Journal of Guidance, Control, and Dynamics*, Vol. 18, No. 4, July–Aug. 1995, pp. 664–673.

[4] Teves, D., Niesl, G., Blaas, A., and Jacklin, S., "The Role of Active Control in Future Rotorcraft," *Proceedings of the 21st European Rotorcraft Forum*, Sept. 1995.

[5] Goodman, R. K., and Millott, T. A., "Design, Development, and Flight Testing of the Active Vibration Control System for the Sikorsky S-92," *Proceedings of the 56th Forum of the American Helicopter Society*, American Helicopter Society, Alexandria, VA, May 2000.

[6] Shaw, J., and Albion, N., "Active Control of the Helicopter Rotor for Vibration Reduction," *Journal of the American Helicopter Society*, Vol. 26, No. 3, Oct. 1981, pp. 32–39.

[7] Cheng, R., Tischler, M. B., and Celi, R., "A High-Order, Time-Invariant Linearized Model for Application to HHC/AFCS Interaction Studies," *Proceedings of the 59th Forum of the American Helicopter Society*, American Helicopter Society, Alexandria, VA, June 2003.

[8] Lovera, M., Colaneri, P., Malpica, C., and Celi, R., "Closed-Loop Aeromechanical Stability Analysis of HHC and IBC, With Application to a Hingeless Rotor Helicopter," *Proceedings of the 29th European Rotorcraft Forum*, DGLR, Bonn, Germany, Sept. 2003.

[9] Wereley, N., and Hall, S., "Linear Control Issues in the Higher Harmonic Control of Helicopter Vibrations," *Proceedings of the 45th Forum of the American Helicopter Society*, American Helicopter Society, Alexandria, VA, 1989.

[10] Lovera, M., Colaneri, P., and Celi, R., "Periodic Control Issues in the Higher Harmonic Control of Helicopter Rotors," *Proceedings of the 2003 American Control Conference*, IEEE, Piscataway, NJ, June 2003.

[11] Theodore, C., and Celi, R., "Helicopter Flight Dynamic Simulation with Refined Aerodynamic and Flexible Blade Modeling," *Journal of Aircraft*, Vol. 39, No. 4, July–Aug. 2002, pp. 577–586.

[12] Celi, R., "Helicopter Rotor Blade Aeroelasticity in Forward Flight with an Implicit Structural Formulation," *AIAA Journal*, Vol. 30, No. 9, Sept. 1992, pp. 2274–2282.

[13] Turnour, S. R., and Celi, R., "Modeling of Flexible Rotor Blades for Helicopter Flight Dynamics Applications," *Journal of the American Helicopter Society*, Vol. 41, No. 1, Jan. 1996, pp. 52–66; editor's correction published in Vol. 41, No. 3, pp. 191–193.

[14] Celi, R., "Implementation of Rotary-Wing Aeromechanical Problems Using Differential-Algebraic Equation Solvers," *Journal of the American Helicopter Society*, Vol. 45, No. 4, Oct. 2000, pp. 253–262.

[15] Celi, R., "Hingeless Rotor Dynamics in Coordinated Turns," *Journal of the American Helicopter Society*, Vol. 36, No. 4, Oct. 1991, pp. 39–47.

[16] Pearson, J. T., and Goodall, R. M., "Adaptive Schemes for the Active Control of Helicopter Structural Response," *IEEE Transactions on Control Systems Technology*, Vol. 2, No. 2, June 1994, pp. 61–72.

[17] Bittanti, S., and Colaneri, P., "Invariant Representations of Discrete-Time Periodic Systems," *Automatica*, Vol. 36, No. 12, Dec. 2000, pp. 1777–1793.

[18] Colaneri, P., Celi, R., and Bittanti, S., "Constant-Coefficient Representations of Periodic-Coefficient Discrete Linear Systems," *Proceedings of the AHS 4th Decennium Specialist's Conference on Aeromechanics*, American Helicopter Society, Alexandria, VA, Jan. 2004.

[19] Rugh, W. J., *Linear System Theory*, 2nd ed., Prentice–Hall, Englewood Cliffs, NJ, 1996, Chap. 20.

[20] Staley, J. A., "Validation of Rotorcraft Flight Simulation Program Through Correlation with Flight Data for Soft-in-Plane Hingeless Rotors," U.S. Army Rept. USAAMRDL-TR-75-50, Ft. Eustis, VA, Jan. 1976.